Journal of Materials Chemistry A

High-χ Diblock Copolymers Containing Poly(vinylpyridine-N-oxide) Segments

Journal:	*Journal of Materials Chemistry A*
Manuscript ID	TA-ART-03-2023-001386.R1
Article Type:	Paper
Date Submitted by the Author:	16-Apr-2023
Complete List of Authors:	Angelopoulou, Polyxeni; Oak Ridge National Laboratory; National and Kapodistrian University of Athens Department of Chemistry Kearney, Logan; Oak Ridge National Laboratory, Chemical Sciences Division Keum, Jong; Oak Ridge National Laboratory, Neutron Scattering Division Collins, Liam; Oak Ridge National Laboratory, Center for Nanophase Materials Science Kumar, Rajeev; Oak Ridge National Laboratory, Center for Nanophase Materials Sciences Sakellariou, Georgios; University of Athens, Chemistry Advincula, Rigoberto; Oak Ridge National Laboratory Center for Nanophase Materials Sciences Mays, Jimmy; The University of Tennessee Knoxville, Chemistry Hong, Kunlun; Oak Ridge National Laboratory, Center for Nanophase Materials Science

High-χ Diblock Copolymers Containing Poly(vinylpyridine-N-oxide) Segments

Polyxeni P. Angelopoulou,[a,b] Logan T. Kearney,[c] Jong K. Keum,[a,d] Liam Collins,[a] Rajeev Kumar,[a] Georgios Sakellariou,[b] Rigoberto C. Advincula,[a] Jimmy W. Mays,*[e] Kunlun Hong *[a]

[a] Center for Nanophase Materials Sciences, Oak Ridge National Laboratory, Oak Ridge, TN 37831, USA

[b] Department of Chemistry, National and Kapodistrian University of Athens, Athens, 15771, Greece

[c] Chemical Sciences Division, Oak Ridge National Laboratory, Oak Ridge, TN 37831, USA

[d] Neutron Scattering Division, Oak Ridge National Laboratory, Oak Ridge, TN 37831, USA

[e] Department of Chemistry, The University of Tennessee, Knoxville TN 37996, USA

Abstract

Block copolymers exhibiting an enhanced segregation strength due to an underlying high Flory–Huggins interaction parameter (high χ) have attracted considerable attention because of their potential of forming microphase-separated domains with very small feature sizes (<10 nm) useful for next-generation lithography. Here, we report the synthesis, characterization, and self-assembly of poly(styrene)-*block*-poly(2-vinylpyridine N-oxide) (PS-*b*-P2VPNO) and poly(styrene)-*block*-poly(4-vinylpyridine N-oxide) (PS-*b*-P4VPNO) block copolymers. These PS-*b*-PVPNOs were obtained from the oxidation of their precursors, poly(styrene)-*block*-poly(2-vinylpyridine) (PS-*b*-P2VP) and poly(styrene)-*block*-poly(4-vinylpyridine) (PS-*b*-P4VP), respectively. The PS-*b*-PVPNOs exhibit an enhanced segregation as revealed by ordered cylindrical and lamellar structures in the sub-10 nm scale from copolymers with relatively low molecular weight. The morphologies and periodicities of the ordered structures were determined by small-angle X-ray scattering, while atomic-force microscopy was used to image the self-assembly in thin films. Estimates of the changes in disorder-order transition temperature and domain spacing are derived from a theory based on the effects of dipolar interactions. All the experimentally observed morphological changes resulting from the oxidation of P2VP and P4VP precursors can be qualitatively explained in terms of an increased dipole moment of

vinylpyridine N-oxide segments. Our results demonstrate that PVPNO based block copolymers are versatile candidates toward nanopatterned structures with small feature sizes critical for the future microelectronics industry and beyond.

1. Introduction

Block copolymers (BCPs) have been extensively studied during the past four decades because of their ability to spontaneously assemble to form a wide range of nanostructures with domain sizes ranging from 2 to 100 nm.[1–3] These self-assembled BCPs have found applications ranging from drug delivery,[4] thermoplastic elastomers,[5] energy conversion and storage,[6–8] separations,[9] to nanolithography.[10,11] For linear block copolymers, the length scales of self-assembled morphologies are dependent on volume fractions of a block (f), total degree of polymerization (N), and the Flory−Huggins interaction parameter (χ) between the two blocks. For flexible diblock copolymers, it has been shown that a critical segregation strength (characterized in terms of χN) is required, $\chi N > 10.5$, for microphase separation. This relationship has been the foundation for harnessing BCP self-assembling phenomena.[3] Furthermore, size of the domains (d) in the strong segregation limit has been predicted to scale as $\chi^{1/6}N^{2/3}$.[12] Hence, an effective strategy to reduce d is to decrease N but keep χ high so that $\chi N > 10.5$ can be maintained.

The need for next-generation lithography patterned polymeric materials has been the driving force in the development of BCP-based self-assembled structures with feature sizes smaller than 10 nm. Typically, the use of BCPs with high-χ and low N is a common strategy to achieve this goal.[13–15] Much work has been done on material design of high-χ block copolymers. Some indicative high-χ systems that have yielded ultra-small feature sizes are poly(styrene)-*block*-poly(glycerol monomethacrylate) (PS-*b*-PGM),[16,17] poly(cyclohexylethylene)-*block*-poly(methyl methacrylate) (PCHE-*b*-PMMA),[18] poly(dimethylsiloxane)-*block*-poly(D,L-lactide) (PDMS-*b*-PLA)[19,20] and poly(4-trimethylsilylstyrene)-*block*-poly(D,L-lactide) (PTMSS-*b*-PLA).[21] A practice often followed is the incorporation of blocks with vast difference in polarity as for example for poly(3-hydroxystyrene)-*block*-poly(dimethylsiloxane) (P3HS-*b*-PDMS),[22] or poly(styrene)-*block*-Poly(hydroxyisobutylene) (PS-*b*-PHIB).[23] The impact of polarity difference on the χ parameter is very well demonstrated in poly(dihydroxystyrene)-*block*-

poly(styrene) (PDHS-*b*-PS), often reported as an ultrahigh-χ system (χ=0.66, 220°C) and allowing for the formation of sub-3 nm nanofeatures.[24] Recently, similar findings on a trihydroxy functionalized polystyrene containing system, poly(trihydroxystyrene)-*block*-poly(styrene) (PTHS-*b*-PS), revealed a remarkable jump in the χ parameter (χ=1.24, 220°C) with ~2 nm half-pitch lamellar structures obtained by ultralow-*N* copolymers.[25] In another recent work, poly(dihydroxystyrene)-*block*-poly(4-trimethylsilylstyrene) (PDHS-*b*-PTMSS) yielded lamellar patterns with 4 nm half-pitch and PTMSS acting both as the hydrophobic block and simultaneously ensuring etch-contrast for nanopatterning applications.[26] During the past few years, the focus on high-χ studies has started shifting to co-oligomers where if the segments have sufficient incompatibility, extremely small ordered nanofeatures on the order of sub-2 nm can be formed.[27,28] Polyzwitterion or ionic blocks have only recently started being incorporated in the hunt for high-χ systems, yielding ultra-small features, and extremely high incompatibilities. Poly(styrene)-*block*-poly(4-vinylpyridine) propane-1-sulfonate (PS-*b*-PVPS), poly(ethylene oxide)-*block*-poly(4-vinylpyridine) propane-1-sulfonate (PEO-*b*-PVPS) and poly(L-lactide)-*block*-poly(4-vinylpyridine) propane-1-sulfonate (PLLA-*b*-PVPS) have been identified as ultrahigh-χ systems,[29] while multiblock copolymers with pendant ionic moieties have led to the extremely high χ value ~3.21 at 25°C and sub-2 nm features.[30]

BCPs containing poly(vinylpyridines) (PVP) segments, including poly(2-vinylpyridine) (P2VP) and poly(4-vinylpyridine) (P4VP), have been intensively studied in the pursuit of high-χ systems and a wide array of self-assembled nanostructures were reported.[31–33] The characteristic structural features in a pyridyl unit renders its unique reactivities and functions. The nitrogen of the pyridyl ring, featuring a lone pair of electrons that do not overlap with the aromatic ring, results in its electron-deficient nature at the carbon positions. The unique reactivities of pyridines and their benzo derivatives can be attributed to the electron-withdrawing, inductive, and mesomeric effects of the nitrogen atom.[34] These effects are more pronounced at C-2 and C-4 positions as compared to the C-3 position. Unlike benzenoid rings in a polystyrene, which is susceptible to electrophilic substitutions, (such as chloromethylation or sulfonation), pyridyl rings in a P2VP or P4VP are generally resistant to electrophilic aromatic substitution but have high reactivities for nucleophilic attacks. The coordination ability of pyridyl rings with various metal ions,

organic/inorganic molecules or building blocks offers a versatile approach to broaden the application of PVP based materials. Moreover, the weak basicity of a pyridyl unit not only facilitates its pH-responsive behavior but also makes it suitable to be derivatized by many reactions, including acylation, alkylation, and N-oxidation.[35] These modified PVPs containing polymers are not only of scientific importance, but also find industrial applications ranging from water treatment, membranes, cosmetics, to biomedicine.[36]

Among various modifications of pyridyl units, N-oxidation (PNO) is an important approach in organic synthesis but much less explored in poly(vinylpyridines). PNO was first reported by Meisenheimer in 1926 and it was commercialized around 1950.[37,38] Compared to its parent molecule, PNO is more nucleophilic and electrophilic with a much large dipole moment (4.37D for PNO vs 2.13D for pyridine).[39,40] Poly(vinylpyridine N-oxide)s (PVPNOs) were synthesized and characterized more than 60 years ago.[41] Their application as a chemotherapeutic agent against silicosis and in preventing the fibrogenesis normally caused by small particles of crystalline silicon dioxide (crystallites) in the lungs of animals and the synthesis of isotope labeled PVPNOs was also reported.[42–45] PVPNOs form complexes with various ions and have been applied as a versatile oxidizing agent for organic compounds.[46] PVPNOs have also been used as polymer-supported oxygen atom transfer reagents and in heterogeneous catalytic reactions.[47,48] The hydrophilic and nonionic properties of PVPNOs in aqueous solutions also facilitate their characteristic interactions with various surfactants.[49] Thus, PVPNOs have been used as additives in laundry detergent to maintain colorfastness.[50] Recently, it was found that PVPNO was a very efficient dye transfer inhibiting (DTI) agent in removing errant dyes by strong electrostatic attraction and shepherding away errant unfixed dyes, resulted in cutting water usage in half, reducing processing time by 75%, and consuming 90% less energy.[51]

To the best of our knowledge, there have been very few BCPs containing PVPNO segments reported.[52] Shevate et al. converted isoporous poly(styrene)-*block*-poly(4-vinylpyridine) (PS-*b*-P4VP) membrane prepared from non-solvent induced phase separation to the corresponding poly(styrene)-*block*-poly(4-vinylpyridine-N-oxide) (PS-*b*-P4VPNO) polyanionic membrane obtained by selective oxidation. The resulted pH responsive PS-*b*-P4VPNO membrane not only conservated the membrane's isoporous structure, but also showed significant improvement in the mechanical and chemical

stabilities.[52,53] Recently, Zeng and co-authors obtained various donor−acceptor noncovalent complexes using poly(4-vinylphenyl chalcogenide) as the donor polymer and poly(ethylene oxide)-*block*-poly(4-vinylpyridine N-oxide) (PEO-*b*-P4VPNO) as the acceptor polymer. These complexes could further aggregate into tubular and spherical assemblies through interchain chalcogen−bonding.[53] PEO-*b*-P4VPNO was synthesized by oxidation of commercial PEO-*b*-P4VP in glacial acetic acid with 30% hydrogen peroxide at 70 ^{o}C for 24 hours. However, the self-assembly behavior of PEO-*b*-P4VPNO was not described. In this contribution, we report the synthesis, characterization, and morphology studies of different poly(styrene)-*block*-poly(vinylpyridine-N-oxide) (PS-*b*-PVPNO) block copolymers. PS-*b*-PVPNO block copolymers were synthesized and their microphase separations featured high-χ characteristics. Our results show that PVPNO based block copolymers have many potential applications including the microelectronics industry (such as next-generation lithography), membrane separation, cosmetics, and sensors.

2. Experimental

2.1. Materials and methods

2.1.1 Materials

Benzene (thiophene free, Sigma-Aldrich), tetrahydrofuran (THF, HPLC grade, Fisher Scientific), hexanes (HPLC grade, Fisher Scientific), methanol (VWR), 2-propanol (VWR), styrene (St, Sigma-Aldrich), styrene-d8 (Sigma-Aldrich), 1,1-diphenylethylene (DPE, Sigma-Aldrich) were purified according to the standards of anionic polymerization high-vacuum techniques as described elsewhere.[54,55] 2-Vinylpyridine (Sigma-Aldrich) and 4-vinylpyridine (Alfa Aesar) were purified by CaH_2, distilled over sodium mirror, then over trioctylaluminum (Sigma-Aldrich) and finally collected through distillation into pre-calibrated ampoules under high-vacuum just prior to polymerization. Glacial acetic acid (Fisher Scientific) and 30% w/v H_2O_2 (Sigma-Aldrich) were used as received.

2.1.2. Methods

PS-*b*-P4VPNO and PS-*b*-P2VPNO block copolymers were prepared by the oxidation of PS-*b*-P4VP and PS-*b*-P2VP parent copolymers. For the determination of the chain

length distributions of the PS-*b*-P4VP and PS-*b*-P2VP precursor copolymers; Size Exclusion Chromatography (SEC) (EcoSEC Elite, Tosoh Bioscience LLC) was utilized. The instrument used was equipped with an RI detector, UV detector, a Tosoh $LenS_3$ Multi-Angle Light Scattering Detector (MALS), and two TSKgel GMH_{HR}-M (L × I.D. 30 cm × 7.8 mm, 5 μm particle size) mixed bed SEC Columns. The columns were housed in a thermostated oven at 55 °C. DMF was the eluent at a flow rate of 0.5 ml/min. For conventional column calibration PS standards in the range of M_p=580-2,227,000 g/mol (from Agilent Technologies) were used.

The composition and average molecular weight of PS-*b*-P4VP and PS-*b*-P2VP were determined by ^{1}H-NMR spectroscopy. NMR spectra were obtained on a Bruker Avance NEO NMR console coupled to a 11.74 T actively shielded magnet (Magnex Scientific/Varian) operating at 499.7 MHz for proton. All spectra were acquired at 298 K in $CDCl_3$ (7.27 ppm ^{1}H reference) or in 1,4-dioxane-d7/D_2O (4.79 ppm ^{1}H reference) or in 1,1,1,3,3,3-Hexafluoro-2-propanol-d_2 (4.52 ppm ^{1}H-reference). Fourier transform infrared spectroscopy (FT-IR) experiments were performed on a Bruker Vertex 70 with a diamond attenuated total reflection (ATR) window in the range of 4000 to 600 cm^{-1}. The peak resolution was set to 4 cm^{-1} and each spectrum was scanned 512 times with air background. Thermogravimetric analysis (TGA) data were collected in the temperature range of 25–700 °C under N_2 flow heated at 20 °C min^{-1} using TA Instruments Discovery TGA. Thermal transition was measured using a TA Instruments (TA Q2000) differential scanning calorimeter (DSC) under a N_2 atmosphere. The reported values (middle point) were from the second heating cycle of a heat/cool/heat procedure. The glass transition temperature (T_g) was determined by TA Universal Analysis software. UV-vis spectroscopy was conducted with a Cary 5000 UV-Vis-NIR spectrophotometer (Agilent Technologies) with a 10 mm optical path quartz cuvette with a 0.001% w/v polymer solution in IPA. Quartz cuvette of same characteristics containing pure solvent was used as the background.

Small-angle X-ray scattering (SAXS) measurements were carried out on a Xenocs Xeuss 3.0 instrument equipped with D2+ MetalJet X-ray source operated at 9.2 keV (Ga Ka, λ = 1.3414 Å). The samples were loaded in the opening of 4 mm-diameter and 0.8 mm-thick steel washers, sandwiched by 0.06 mm-thick Kapton films, and aligned perpendicular to the direction of the X-ray beam (transmission mode). The scattered beam was recorded

on a Dectris Eiger 2R 4M hybrid photon counting detector with a pixel dimension of 75 × 75 μm^2. The sample-to-detector distance for SAXS was calibrated using Silver Behenate (AgBeh) standard, which was 1750 mm, and the exposure time was 360 s. Before annealing, oxidized block copolymer samples were compression molded at 150 ^{o}C for 20 min inside the steel washers, capped on one side with Kapton film and exposed to solvent vapors in a 500 cm^3 closed container containing 30 ml of solvent (*p*-dioxane/water 70/30 v/v) for 12 h at RT in order to perform solvent vapor annealing (SVA) followed by drying at ambient conditions for 30 hours. For some measurements, thermal annealing for 24 hours at 160 ^{o}C in a vacuum oven was also conducted after the SVA process. The precursor block copolymers PS-*b*-P4VP and PS-*b*-P2VP were thermally annealed at 160 ^{o}C (above the glass transition temperatures of both blocks, for 24 hours under vacuum. The collected 2-dimensional (2D) SAXS images were circularly averaged and expressed as intensity *versus* scattering vector q, where $q = (4\pi \sin \theta)/\lambda$ with θ and λ being the half of scattering angle and X-ray beam wavelength. All the data were corrected for detector background. For temperature-dependent SAXS, a custom-made Linkam DSC hot stage was used with 10 ^{o}C/min heating rate, 360 s exposure time and 5 min equilibration time at each temperature.

Atomic force microscopy (AFM) of block copolymer thin films was conducted on a Cypher (Asylum Research) AFM Microscope in a tapping mode using Si cantilevers (Bruker, TESPA-V2) with 7 nm tip radius and ~320 kHz resonance frequency. Thin films of dPS-*b*-P2VPNO were prepared on 1 cm^2 Si UV/O^3 treated wafers by spin coating. The thin films were annealed by SVA for 18 hours by exposing to solvent vapors in a 500 cm^3 closed container containing 30 ml of solvent (*p*-dioxane/water 70/30 v/v). After 8 hours of drying at ambient conditions, thermal annealing at 140 ^{o}C for 12 hours followed.

2.2. Synthetic procedures

2.2.1 PS-*b*-P2VP and PS-*b*-P4VP block copolymers (Table 1) were synthesized according to reported procedures. Details of these syntheses are listed in the ESI section.

2.2.2 Synthesis of PS-*b*-P2VPNO and PS-*b*-P4VPNO

PS-*b*-P2VPNO and PS-*b*-P4VPNO were synthesized from their respective precursors following a slightly modified procedure reported by Ochiai [56] as shown in Scheme 1. In a typical procedure, 1.5 grams of PS_{34}-*b*-$P2VP_{25}$ diblock copolymer (pyridyl units 6.13

mmol) were suspended in glacial acetic acid (10 mL) and 30% H_2O_2 (1.3 mL, 11.56 mmol) was added.[57] The mixture was left to stir at 75 °C for 24 hours under an inert atmosphere. Then, the mixture was evaporated to dryness, neutralized with aqueous NaOH solution, and further purified by dialysis against DI water (MWCO=1 kDa). After freeze-drying the oxidized copolymer was obtained as a slightly yellow powder. Other block copolymers were oxidized using the same protocol and details for these polymers were listed in Table 1.

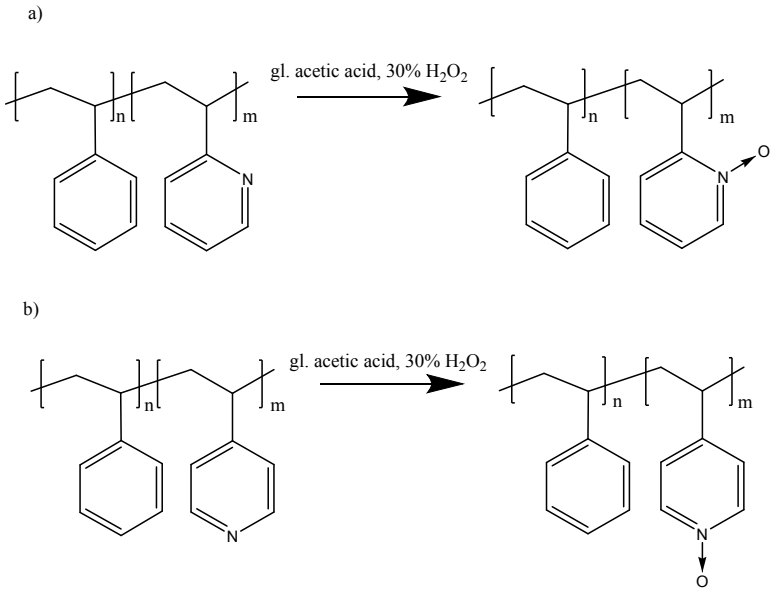

Scheme 1. Synthetic schemes for a) PS-*b*-P2VPNO, b) PS-*b*-P4VPNO diblock copolymers.

3. Results and Discussion

3.1 Synthesis of PS-*b*-P4VP, PS-*b*-P2VP diblock copolymers

PS-*b*-P2VP and PS-*b*-P4VP block copolymers were synthesized by sequential anionic polymerizations under high-vacuum using break-seal techniques. Details of the synthesis can be found in ESI section. The characteristics of the block copolymers used in the following studies are summarized in Table 1. The compositions of the block copolymers were determined by ^{1}H-NMR using the integration of the peak at 6-7.2 ppm where the five aromatic protons of PS and two protons of P4VP or three protons of P2VP appear, alongside the integration of the peak at 8-8.5 ppm where two protons of P4VP or one proton

of P2VP appear in ^{1}H-NMR in $CDCl_3$. A typical spectrum is shown below (Fig. 1). For PS-*b*-P2VP and PS-*b*-P4VP samples, quantitative ^{1}H-NMR was used for molecular weight (M_n) determination. The three methyl protons of *n*-BuLi (in the case of PS-*b*-P4VP) or the six methyl protons of *sec*-BuLi (in the case of PS-*b*-P2VP) at 0.5-0.8 ppm were used. To confirm the correct assignment of this peak to the methyl protons of the initiator, Heteronuclear Single Quantum Coherence (HSQC) spectroscopy was used (Fig. S3). With the 2-D NMR experiment the correlation of the ^{13}C and ^{1}H nuclei allowed to confirm the correct peak assignment. By using HSQC, the integrity of molecular weight and degree of polymerization (*N*) determination by ^{1}H NMR using the methyl peaks of the initiator was confirmed. Important peaks such as the peak at 0.8 ppm assigned to the methyl protons of the initiator (6H for *sec*-BuLi, 3H for *n*-BuLi) with 2D-HSQC are better resolved and these protons are clearly correlated to the methyl ^{13}C. For dPS-*b*-P2VPNO, M_n, composition, and the dispersity of the copolymers was determined by size exclusion chromatography (SEC). Typical SEC traces are shown in Fig. 2, 3. The volume fractions of the PS block for each copolymer was measured using the mass composition and densities of each block at room temperature $f_A = w_A\rho_B/[w_A\rho_B+(100-w_A)\rho_A]$. Known densities of PS, P2VP, P4VP ρ_{PS}=1.05 g/cm^3, ρ_{dPS}=1.15 g/cm^3, ρ_{P2VP}=1.14 g/cm^3, ρ_{P4VP}=1.11 g/cm^3 were used.[58,59] The densities of P2VPNO, P4VPNO ρ_{P2VPNO}=1.14 g/cm^3, ρ_{P4VPNO}=1.16 g/cm^3 were determined by pycnometry at RT (details in ESI). The total degrees of polymerization (*N*) are volume-based averaged using a reference volume $v_{0=}$118Å^3 according to the formula $N=M_n/(\rho N_A v_0)$.

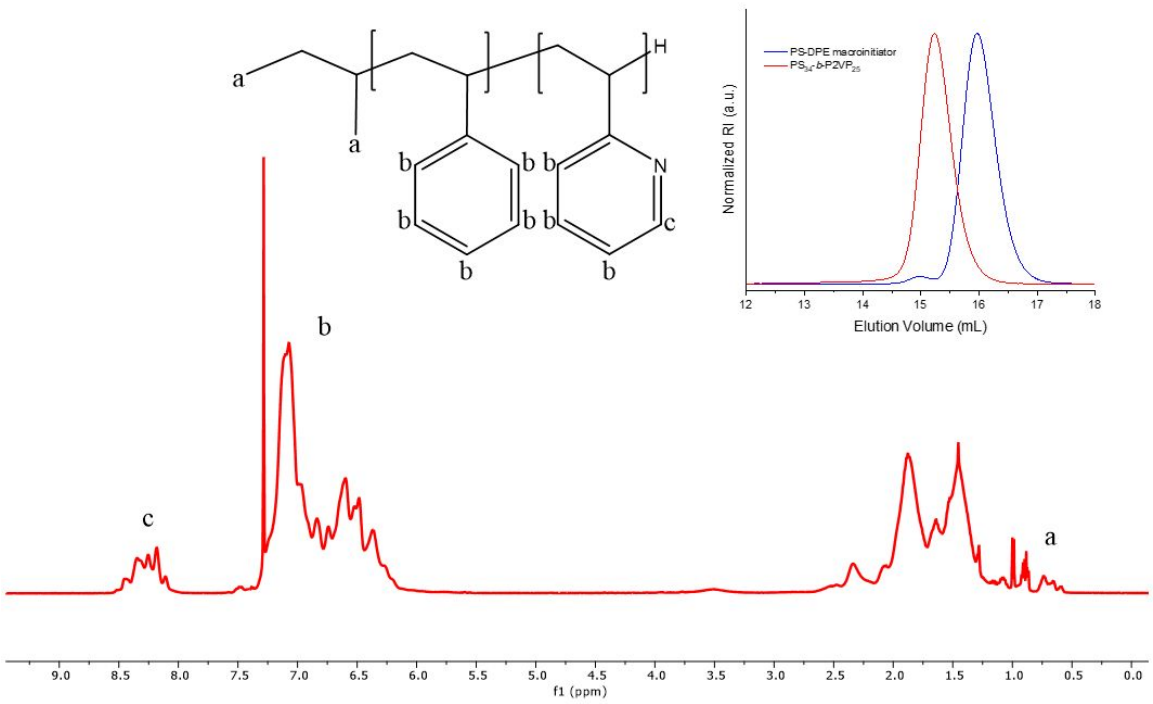

Figure 1. ^{1}H NMR spectrum in $CDCl_3$ of PS_{34}-*b*-$P2VP_{25}$ showing relevant peak assignments. Inset: SEC chromatogram of PS-DPE macroinitiator (blue) and the chain-extended PS_{34}-*b*-$P2VP_{25}$ (red) (3.5K-2.6K)

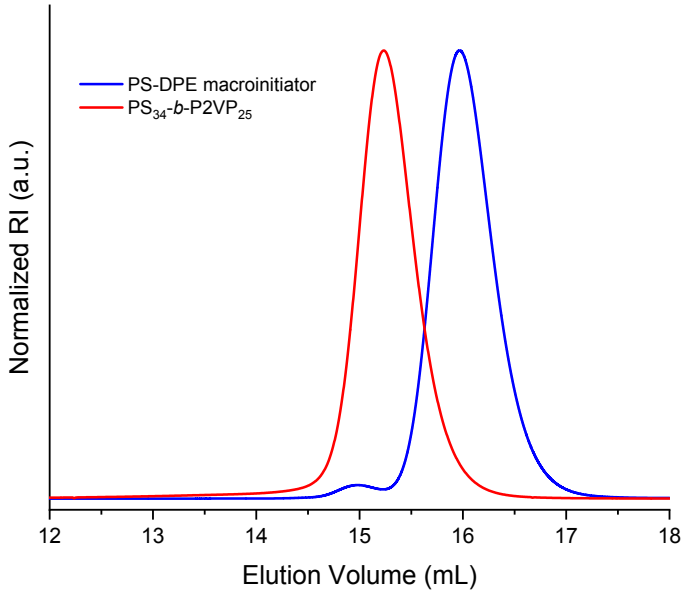

Figure 2. SEC chromatograms of PS-DPE macroinitiator and respective PS_{34}-*b*-$P2VP_{25}$ diblock copolymer. PS-DPE was polymerized in benzene, while P2VP was polymerized in a mixture solvent (benzene/THF).

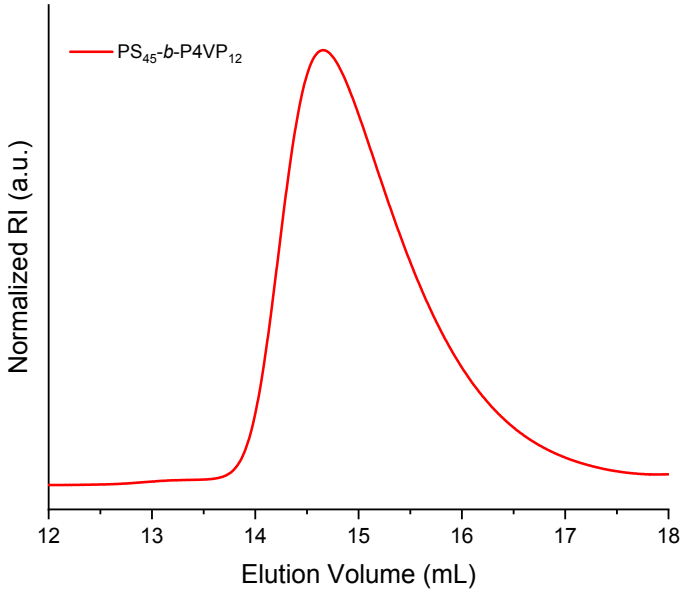

Figure 3. SEC chromatogram of PS_{45}-*b*-$P4VP_{12}$ diblock copolymer. For this copolymer both blocks were polymerized in THF. An aliquot of the macroinitiator was not able to be collected due to concerns about pyrolysis of this solvent.

Table 1. Molecular characteristics of precursor diblock copolymers

Sample	Total M_n [a] (g/mol)	$Đ$ [b]	N_{PS} [a]	N_{PVP} [a]	$N_{Tot}^{118Å^3}$ [c]	f_{PS} [d]
PS_{45}-*b*-$P4VP_{12}$	6.0K	1.50	45	12	79	0.79
PS_{34}-*b*-$P4VP_{27}$	6.3K	1.27	34	27	82	0.56
PS_{34}-*b*-$P2VP_{12}$	4.8K	1.06	34	12	63	0.75
PS_{34}-*b*-$P2VP_{25}$	6.1K	1.10	34	25	79	0.59
dPS_{77}-*b*-$P2VP_{76}$	16.0K [b]	1.09	77	76	197	0.52

[a] Determined by ^{1}H-NMR

[b] Determined by SEC in DMF

[c] Volume-based averaged, with a reference volume $v_{0=}118Å^3$

[d] Calculated based on the mass composition and the block densities

3.2 Synthesis of PS-*b*-P2VPNO and PS-*b*-P4VPNO diblock copolymers

The oxidation of the copolymers was conducted by using glacial acetic acid and H_2O_2. The mechanism involves the formation of peroxyacetic acid.[56,60] The oxidized analogues (P4VPNO and P2VPNO) exhibit two distinct bands at ~1170 and 1230 cm^{-1} in FTIR, corresponding to oxygen bending vibration and N^+-O^- stretching vibration of N^+-O^- (Fig. 4, 5, S4).[52]

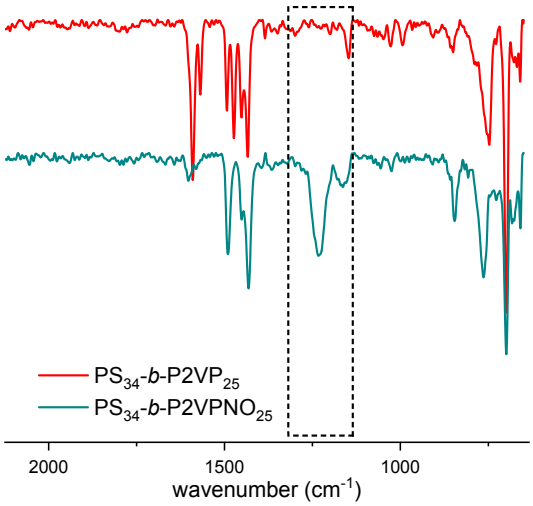

Figure 4. ATR-FTIR spectra of PS_{34}-*b*-$P2VP_{25}$ (red) PS_{34}-*b*-$P2VPNO_{25}$ (dark green). The bands at 1170 and 1230 cm^{-1} corresponding to oxygen bending vibration and N^+-O^- stretching vibration of N^+-O^- are prominent after the oxidation.

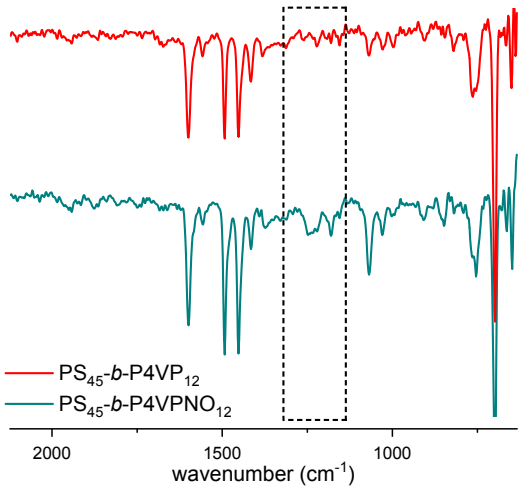

Figure 5. ATR-FTIR spectra of PS_{45}-*b*-$P4VP_{12}$ (red) PS_{45}-*b*-$P4VPNO_{12}$ (dark green). The bands at 1170 and 1230 cm^{-1} corresponding to oxygen bending vibration and N^+-O^- stretching vibration of N^+-O^- are prominent after the oxidation.

In addition, UV-Vis spectra (dilute solution in 2-propanol) revealed that the unoxidized PS-*b*-P2VP exhibits a band at λ_{max}=263 nm with evident shoulders. (Fig. 6, S8) After

oxidation the absorption band shifts to λ_{max}=270nm and these shoulders disappear completely, indicative of the quantitative oxidation. Similar behavior is observed for the oxidation of PS-*b*-P4VP where before oxidation a band at λ_{max}=256 nm with evident shoulders is observed. After its oxidation the absorption band shifts to λ_{max}=270 nm and these shoulders again disappear. It is noteworthy that P4VPNO is not well-soluble in 2-propanol.[44,57,61–63] In spite of the large difference in the solubility of poly(vinylpyridine)s upon oxidation, we tried to identify a common solvent for the precursor and oxidized homopolymers to conduct comparative NMR experiments. From these measurements is evident that the peak associated with the protons in the ortho position of poly(vinylpyridine)s shifts downfield upon oxidation. Although this shift is not big, it can still be seen that no residual peak associated with the parent material is observed. These data are included in the ESI section (Fig. S9-S13).

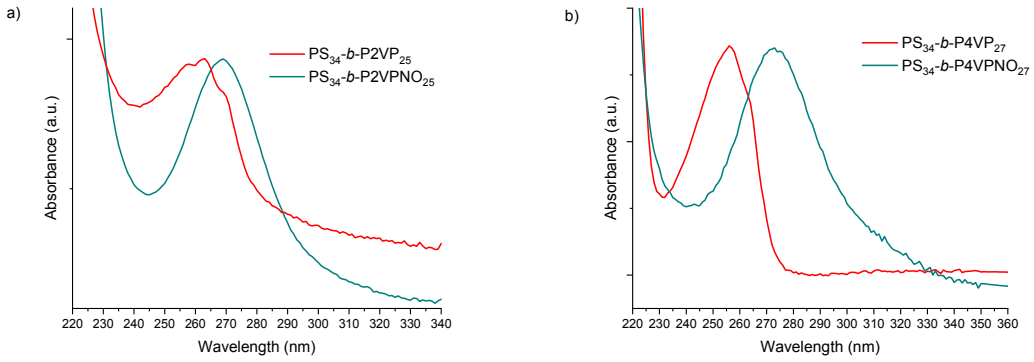

Figure 6. a) UV-Vis spectra of PS_{34}-*b*-$P2VP_{25}$ (red) and PS_{34}-*b*-$P2VPNO_{25}$ (dark green) in IPA. b) UV-Vis spectra of PS_{34}-*b*-$P4VP_{27}$ (red) and PS_{34}-*b*-$P4VPNO_{27}$ (dark green) in IPA. Upon oxidation the band at λ_{max}=270 nm appears symmetric and without the shoulders observed before oxidation.

Both homopolymers and copolymers bearing PVPNO blocks, along with the unoxidized precursors, were characterized by DSC and TGA. (Fig. 7 and Fig. S14-S21) There was no evident glass transition temperature *(T_g)* determined for P2VPNO or P4VPNO homopolymers at temperatures lower than their decomposition temperature (T_d) (see Information in ESI Fig. S14, S15).[64] Similar behavior was reported for polyzwitterions. In this case, it is considered that the zwitterionic side-groups of the

polymer impart inter- and intra- molecular interactions of dipole-dipole character. These kinds of interactions, serving as physical crosslinks, provide improved mechanical strength while lead to lack of glass transition relaxation before degradation during conventional DSC measurements.[65]

The parent block copolymers in our study (PS-*b*-P4VP, PS-*b*-P2VP and dPS-*b*-P2VP) mostly exhibited a single T_g, indicating the miscibility between the low molecular weight blocks of these copolymers. After oxidation, a single T_g was observed in all block copolymers but with higher values, indicating segmental mobility is restrained after the oxidation of the PVP block.[52] We believe that the glass transition of the oxidized blocks was not observed within the temperature range of the conventional DSC measurement because of the very high T_g of the oxidized poly(vinylpyridine)s. It is worth to note here that SAXS data showing immiscible segments exhibiting phase separation were observed for all oxidized block copolymers as will be discussed further in a following section.

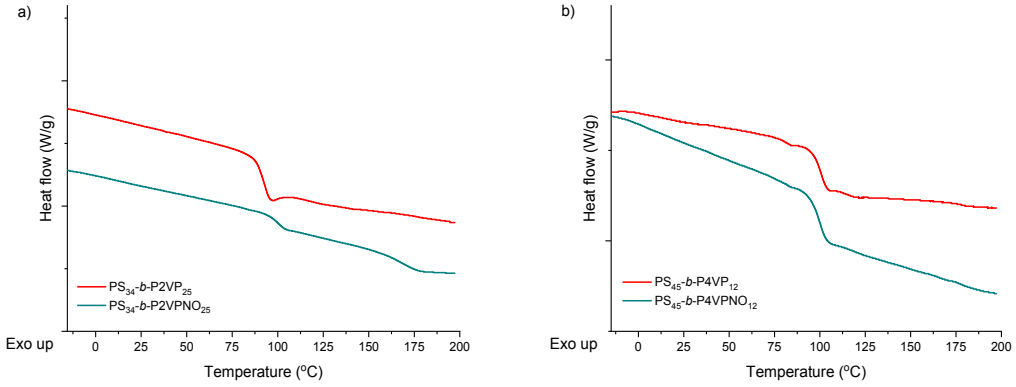

Figure 7. a) DSC thermograms of precursor PS_{34}-*b*-$P2VP_{25}$ (red) and oxidized PS_{34}-*b*-$P2VPNO_{25}$ (dark green) block copolymer. b) DSC thermograms of precursor PS_{45}-*b*-$P4VP_{12}$ (red) and oxidized PS_{45}-*b*-$P4VPNO_{12}$ (dark green) block copolymer.

3.3 Self-assembly of PS-*b*-P4VPNO and PS-*b*-P2VPNO

3.3.1 SAXS studies

High Flory-Huggins parameters (χ) are expected for PVPNO and PS block copolymers because of the considerable difference of polarity between the two monomeric units. Thus,

phase separation of PS-*b*-PVPNOs block copolymers should occur even at relatively low molecular weight. To examine the bulk block copolymer self-assembly, both precursors (PS-*b*-P4VP, PS-*b*-P2VP, dPS-*b*-P2VP) and their oxidized derivatives (PS-*b*-P4VPNO, PS-*b*-P2VPNO, dPS-*b*-P2VPNO) were carefully characterized by SAXS. The precursors were thermally annealed at 160 ^{o}C for 24 hours. Two different annealing procedures were followed for the oxidized copolymers PS-*b*-P4VPNO, PS-*b*-P2VPNO, dPS-*b*-P2VPNO analogues prior to SAXS measurements. In the first procedure, solvent vapor annealing (SVA) in a mixture of *p*-dioxane/water 70/30 (v/v) for 12 hours with subsequent slow drying for 30 hours was performed. (Fig. 8-10) Immediately after the exposure to solvent vapors, the samples were found to be substantially swollen, while upon the slow deswelling, glassy, brittle, thick films were obtained. *p*-Dioxane is a good solvent for PS, while water is a good solvent for PVPNOs and the two solvents have similar boiling points. This solvent system was chosen to ensure that both blocks will swell sufficiently for the chains to get mobilized and phase separated, since PVPNOs exhibit glass transition temperatures higher than their degradation temperatures. Small-angle X-ray scattering data obtained after this annealing procedure are summarized in Table 2.

This kind of annealing, however, is affected by multiple variables, such as relative humidity, temperature, block selectivity, evaporation rate, degree of swelling, among others. Particularly the selectivity of the solvent vapors towards one block, can lead to altered effective volume fraction (f_{eff}) and respective shift in phase boundaries, while changes in domain periodicities can also be observed.[66,67] Because of this and in order to get a better insight into the phase behavior of the copolymers, a second two-step annealing process was also explored. (Fig. S24) In the first step, SVA was conducted followed by 24 hours of thermal annealing at 155 ^{o}C under vacuum. During this second step of annealing, any traces of solvent should be removed, while the chains get partially relaxed as the temperature is higher than the T_g of PS. Similar annealing procedures have been reported by others investigating highly-immiscible charge-bearing block copolymers.[29]

Before oxidation, disordered structures occur for most precursor copolymers. On the contrary, after the oxidation high-χ copolymers with well-ordered structures, and small periodical dimensions, despite the low degrees of polymerizations (low-*N*), are obtained. When both precursor and final copolymers form ordered structures, as in the case of PS_{34}-*b*-

$P4VP_{27}$ and PS_{34}-*b*-$P4VPNO_{27}$, the domain spacing, d, is larger after the oxidation since d scales not only with the degree of polymerization (N), but also with the χ parameter ($d \sim \chi^{1/6} N^{2/3}$). This implies that the χ parameter increased after the oxidation. Slightly different domain-spacings were observed from the two different annealing procedures, with the periodicities being smaller in the case where both SVA and thermal annealing was followed. It is believed that this is because of solvent traces remaining in the bulk film and swelling the domains without subsequent thermal treatment. For one sample, PS_{45}-*b*-$P4VPNO_{12}$, the coexistence of both lamellae and cylinders was observed when only SVA was used. (Fig. 8) After further thermal annealing, only lamellar structures were obtained for this copolymer (details discussed below). It should, also, be mentioned that after thermal annealing the peaks for most of the samples appear less sharp, indicative of a compromise in ordering. (Fig. S24)

Table 2. Block copolymer structural and morphological characteristics

Sample	Annealing[a]	N_{PS}[b]	N_{PVP}[b]	f_{PS}	Morphology[c]	d (nm)[d]
PS_{45}-*b*-$P4VP_{12}$	TA	45	12	0.79	Lamellae	12.6
PS_{45}-*b*-$P4VPNO_{12}$	SVA	45	12	0.78	Lamellae/Cylinders	(L)19.1/(C)15.6
	SVA & TA				Cylinders	15.5
PS_{34}-*b*-$P4VP_{27}$	TA	34	27	0.56	Lamellae	13.9
PS_{34}-*b*-$P4VPNO_{27}$	SVA	34	27	0.53	Cylinders	19.9
	SVA & TA				Cylinders	17.3
PS_{34}-*b*-$P2VP_{25}$	TA	34	25	0.59	Disordered	-
PS_{34}-*b*-$P2VPNO_{25}$	SVA	45	12	0.56	Lamellae	13.6
	SVA & TA				Lamellae	12.3

[a] The precursor PS-*b*-PVP were thermally annealed (TA). The oxidized analogues, annealed by Solvent Vapor Annealing (SVA) only or by SVA followed by thermal annealing (i.e., SVA & TA) as described in section 2.1.2.

[b] Determined by ^{1}H-NMR.

[c] The morphology was determined by the scattering peaks ratio with respect to the primary scattering peak, q*.

[d] d=2π/q*: Thermal annealing for parent copolymers, Solvent Vapor Annealing for oxidized copolymers.

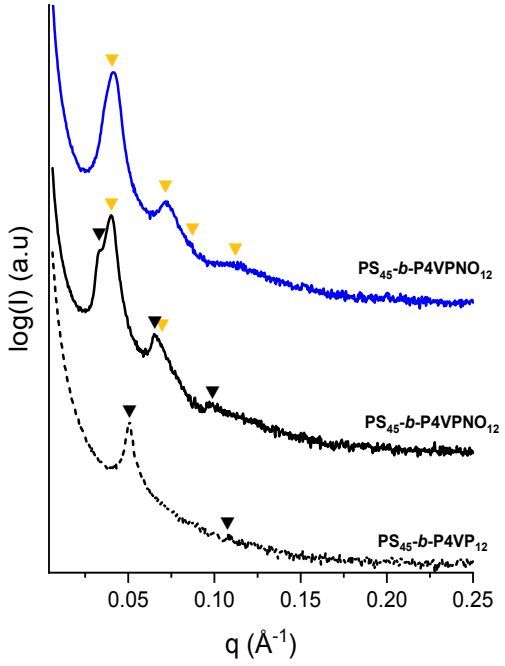

Figure 8. Room Temperature SAXS spectra of precursor PS_{45}-*b*-$P4VP_{12}$ block copolymer thermally annealed (black dashed line) and oxidized PS_{45}-*b*-$P4VPNO_{12}$ block copolymers annealed by SVA (black solid line) or annealed by SVA and subsequent TA (blue solid line). The black arrows refer to scattering peaks in the sequence of 1:2:3:4 indicative of lamellar structures, while the orange arrows refer to scattering peaks in the sequence of 1:√3:2 indicative of cylindrical structures.

In Fig. 8, it is clearly shown that PS_{45}-*b*-$P4VP_{12}$ (M_n=6.0K, f_{PS}=0.79) diblock copolymer exhibits a sharp 1st order peak and faint but discernable 2nd order peak, indicating the lamellar morphology. After oxidation, multiple scattering peaks are observed. It is interesting to notice that different morphological behavior was observed when different annealing procedures were applied for the oxidized analogue (PS_{45}-*b*-

P4VPNO$_{12}$). When only SVA was used, peaks relevant to both lamellar and cylindrical structures were observed. The apparent volume fraction of the PS$_{45}$-*b*-P4VPNO$_{12}$ possibly lied on the phase boundaries between cylindrical and lamellar phases under the solvent vapor annealing conditions used. If traces of the annealing solvent system may be held by one of the domains in the copolymer, this could have led to altered f_{eff} and thus the coexistence of different morphologies. Once thermal annealing took place and the solvent was removed, only cylindrical structures were observed. (Fig. 8, S24) To investigate the effect of solvent swelling on the morphologies attained, a three-step annealing procedure (1. SVA, 2. TA, 3. SVA) was carried out. Indeed, after the third annealing step, coexistence of the cylindrical and lamellar morphologies reoccurred and confirmed that the presence of solvent in the sample and/or the swelling driven by the solvents affect the phase behavior by changing the apparent volume fraction of the phase diagram of the BCP system. (Fig S25)

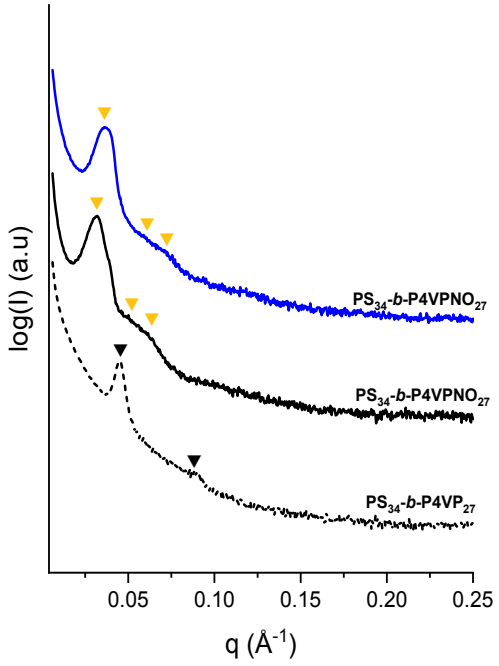

Figure 9. Room Temperature SAXS data of precursor PS$_{34}$-*b*-P4VP$_{27}$ block copolymer thermally annealed (dashed line) and oxidized PS$_{34}$-*b*-P4VPNO$_{27}$ block copolymers annealed by SVA (solid line) or annealed by SVA and subsequent TA (blue solid line). The black arrows refer to scattering peaks in the sequence of 1:2:3 indicative of lamellar

structures, while the orange arrows refer to scattering peaks in the sequence of 1:√3:2 indicative of cylindrical structures.

For PS_{34}-*b*-$P4VP_{27}$ with symmetric composition (M_n=6.3K, f_{PS}=0.56), lamellar structures with d=13.9 nm were observed after thermal annealing as expected. For its oxidized analogue (f_{PS}=0.53), hexagonal close packed cylinders with d=19.9 nm were observed after SVA. When SVA was followed by TA, the morphology was again HCP cylinders this time with d=17.3 nm. (Figure 9). The increased d-spacing after the oxidation showed the large χ in this block copolymers. The fact that different morphologies were obtained by the oxidized and non-oxidized copolymer, is an indication of the increased elasticity asymmetry after oxidation. Before the oxidation, the almost compositionally symmetric copolymer gives the predicted lamellar structures. However, after the oxidation and despite the volume fraction corresponding to a more symmetric copolymer, the attained morphology is HCP cylinders. We believe that in this case the cylinders consist of the more flexible PS blocks whereas the matrix consists of the more rigid P4VPNO segments. In this sample, the peaks are relatively broad making the peak positions not so pronounced.

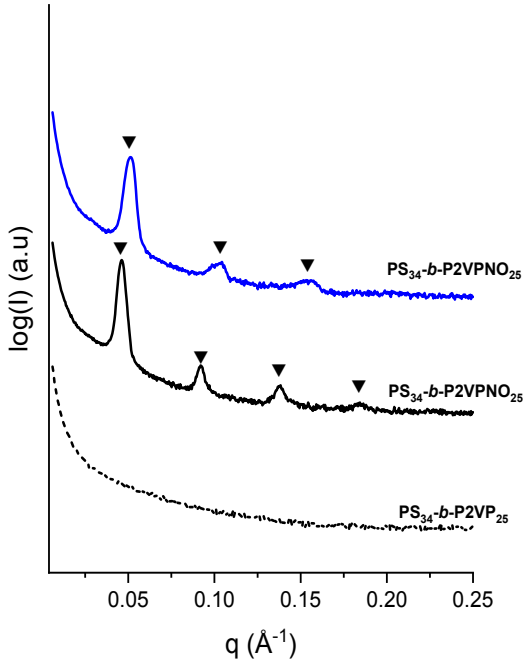

Figure 10. Room Temperature SAXS data of precursor PS_{34}-*b*-$P2VP_{25}$ block copolymer thermally annealed (dashed line) and oxidized PS_{34}-*b*-$P2VPNO_{25}$ block copolymers annealed by SVA (solid line) or annealed by SVA and subsequent TA (blue

solid line). The black arrows refer to scattering peaks in the sequence of 1:2:3:4 indicative of lamellar structures.

For a P2VP based block copolymer (PS_{34}-*b*-$P2VP_{25}$), no peaks were observed before the oxidation because of the miscibility of the two blocks. After oxidation, multiple peaks (q*:2q*:3q*:4q*) up to 4th order were clearly observed indicating well-ordered lamellar domains when solvent vapor annealing (SVA) was followed. (Fig. 10) Well-defined periodical two-phase morphology of which d-spacing equal to 13.6 nm (half-pitch 6.8 nm) highlighted a large degree of immiscibility of the two blocks, sufficient for phase separation in such low molecular weight (M_n=6.3K, f_{PS}=0.54) copolymers. When SVA and subsequent thermal annealing was conducted for PS_{34}-b-$P2VPNO_{25}$, the peaks appeared to be slightly broader while exhibiting peaks up to 3rd order with one peak less as compared to the SVA-only annealing. Additionally, the domain spacing was slightly smaller (~12.3 nm). (Fig. 10, S24) Temperature-dependent SAXS was also conducted for PS_{34}-*b*-$P2VPNO_{25}$ using a customized Linkam DSC stage. Despite increasing the temperature up to 220 ^{o}C, all scattering peaks were preserved. (Fig. S26) This is a clear indication of the high level of ordering taking place due to the large immiscibility between the blocks, despite the low molecular weight nature of the copolymer.

For compositionally asymmetrical PS_{34}-*b*-$P2VP_{12}$, the parent block copolymer (M_n=4.8K, f_{PS}=0.75) shows no phase separation without any ordered peaks. (Fig. S24) Upon oxidation (f_{PS}=0.72) and after SVA, the block copolymer exhibits two peaks at q* and √3q*, indicative of 2D hexagonal close packed cylinders with d_{10}-spacing=9.7 nm. This is the smallest *d*-spacing observed in this study because the high immiscibility (high χ) among the blocks allowed the phase separated structures preserved even for low-M_n. When the oxidized copolymer is annealed thermally after the SVA, the second-order peak disappears.

We also studied a higher molecular weight block copolymer with the PS block deuterated (dPS_{77}-*b*-$P2VP_{76}$) and its corresponding oxidized derivative (dPS_{77}-*b*-$P2VPNO_{76}$ **(**Fig. S27 and Fig S24) The parent block copolymer (dPS_{77}-*b*-$P2VP_{76}$, M_n=16.0K, f_{dPS}=0.52) showed a primary scattering peak along with a second order peak appear at q*:2q* position after thermal annealing, implying lamellar morphology with domain periodicity of 16.5 nm. After oxidation (f_{PS}=0.48), the resulted dPS_{77}-*b*-$P2VPNO_{76}$

exhibited ordered peaks corresponding to cylindrical structures with d=26.0 nm after SVA. The morphology remained the same, but peaks appeared to be less sharp, with the two-step annealing (SVA, thermal annealing). It is noteworthy that different morphologies appeared after the oxidation, which further demonstrated the higher elasticity asymmetry after the modification of the pyridyl blocks. The large increase in domain periodicity after the oxidation can be attributed to an increased χ parameter, where the factor $\chi^{1/6}$ in the equation $d \sim \chi^{1/6} N^{2/3}$ became significant resulting in increased *d*-spacing. The thin film structure of this sample was confirmed by AFM as discussed in the following section. It is worth noting that in this block copolymer cylindrical structures formed, although the volume fraction was similar to PS_{34}-*b*-$P2VPNO_{25}$ where lamellar structures observed. We believe that this copolymer lies on the border between lamellar and cylindrical phases, despite being symmetric due to higher segregation strength and the elasticity asymmetry effect.

3.3.2 AFM study

The self-assembly of dPS_{77}-*b*-$P2VPNO_{76}$ was studied in thin-films by AFM. After annealing the thin-film with similar conditions as for the bulk samples (1.SVA, 2.TA), HCP cylinders mostly lying parallel to the substrate appeared. In certain regions, however, circular cross-section with 2D hexagonal packing appeared, indicating the existence of cylinders lied perpendicular to the substrate surface. On Si-substrate, due to the anisotropic nature of 2D cylinder, the preferred orientation should be the parallel orientation to the substrate rather than the vertical. This is, also, often observed in high-χ systems due to the difference in surface energies of the copolymers. (Fig. 11, Fig. S27)

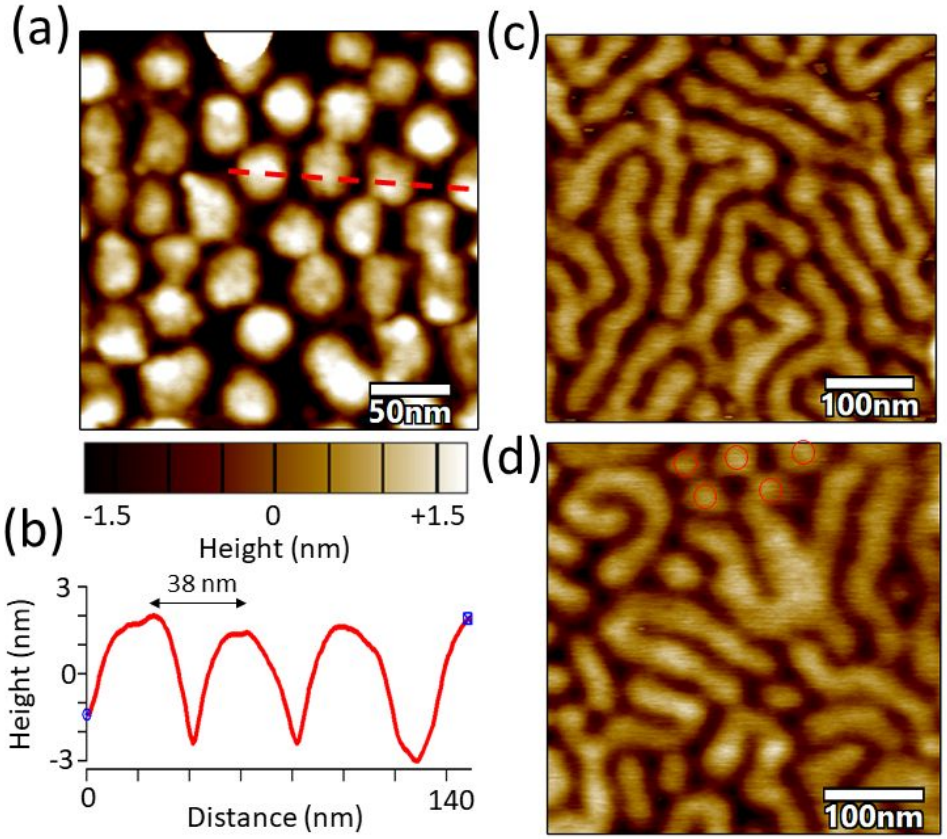

Figure 11. (a,b) AFM image and respective crosse-section indicating vertical to the substrate hexagonal close packed cylinders, (c,d) AFM images of HCP cylinders with parallel to the substrate orientation. All images capturing different regions of the same silicon wafer coated with dPS_{77}-*b*-$P2VPNO_{76}$. In this sample, cylinders with mixed orientations are observed.

The center-to-center distance between two neighboring cylinders was determined to be 38 nm. This is slightly higher than the dimensions we would expect from the SAXS data (Fig. S) ($\frac{2}{\sqrt{3}}$ x d= 32 nm). However, errors due to tip convolution should be taken into consideration as they can affect the measured domain dimensions. Similarly, phase behavior can be altered when bulk versus thin-film samples are examined.

3.3.3 Estimate of Flory-Huggins parameters

The estimation of χ parameter is of paramount interest for block copolymer self-assemblies, especially for systems where high immiscibility is required among the blocks to maintain phase-separated structures with low molecular weight copolymers (high-χ, low-N). Several methods have been established to obtain or predict the χ parameter. Most successful techniques rely on mean-field theories based on concentration fluctuations extracted by SAXS and/or SANS techniques.[1,68,69] Often the scattering profiles in the disordered state are fitted using Leibler's theory and modified to include dispersity effects and asymmetry in the segmental volume effects, to obtain χ as a function of temperature. Another method depends on the mean-field theory assumption that the order-disorder transition for a symmetric linear diblock copolymer occurs at χN=10.5. Thus, by measuring the T_{ODT} for multiple symmetric copolymers, the temperature dependence of χ can be determined.[70] To identify the order-disorder transition temperature SAXS, SANS, or dynamic mechanical measurements are used. Another method to evaluate χ rely on the so-called solubility parameter formalism where χ is expressed as a function of the solubility parameter (δ) difference between the blocks.[68,71] Estimations based on the domain spacing (d) dimensions in phase separated block copolymers in the strong segregation limit, have also been used to evaluate the Flory-Huggins interaction parameter.[20] Other methods, using polymer blends have been explored as well.[72,73] Since different methods rely on different principles and approximations, the χ value of a particular block copolymer system can deviate depending on the evaluation method used.

For the block copolymers studied here, we did not observe order-disorder transition temperatures. Thus, it was not possible to extract χ parameters using the methods discussed above. However, we can estimate temperature dependence of the χ parameter, and resulting changes in disorder-order transition temperature as well as domain spacing using a recently proposed theory of microphase separation in diblock copolymers.[74] The theory predicts the effects of permanent dipoles in affecting the χ parameter and resulting changes in microphase separation. For an AB diblock containing permanent dipoles of length p_A and p_B along A and B segments, respectively, the theory predicts $\chi = \chi_0 + \frac{p^4}{16\pi\rho_0 b^3}$, where $p^2 = \frac{4\pi l_{B0}\rho_0}{3}\left(p_A^2 - p_B^2\right)$ and $l_{B0} = \frac{e^2}{4\pi\epsilon_0 k_B T}$ is the Bjerrum length in vacuum so that e is the charge of an electron, ϵ_0 is permittivity of vacuum, k_B is the Boltzmann constant, T is the

temperature (in Kelvin), $\rho_0 = 1/v_0$ is the segment number density, v_0 is the volume of a segment and b is the Kuhn segment length. Here, χ_0 is the chi parameter in the absence of permanent dipoles and it should be clear that an increase in mismatch between the dipole moments of two kinds of segments will lead to an increase in χ, which agrees with "polar-likes-polar" empirical rule. Taking an A segment to represent polar block like vinyl pyridine and its oxidized N-oxidized block, and B to represent non-polar styrene (i.e., $p_B = 0$), we can estimate temperature dependence of the χ parameter and the effects of oxidation on disorder-order transition (DOT) temperature. Oxidation of vinyl pyridine groups lead to an increase in dipole moment of a segment from ~2.13 D ($p_A = 0.045\ nm$) to ~ 4.37 D ($p_A = 0.092\ nm$). This implies that $\chi_{P2VP-PS} = \chi_0 + (\frac{169.2}{T})^2$ and $\chi_{P2VPNO-PS} = \chi_0 + (\frac{707.2}{T})^2$, where we have used $v_0 = b^3 = 0.118\ nm^3$. We should point out that χ_0 can depend on temperature as well just like in many non-polar diblock copolymers. This in turn, doesn't allow us to make quantitative predictions about DOT and domain spacing in the strong segregation limit. Nevertheless, we can estimate effects of oxidation on DOT by using a result derived in reference 74. In particular, DOT is given by $\chi_0 + \frac{p^4}{16\pi\rho_0 b^3} = \frac{10.5}{N} + \frac{1}{Nf(1-f)}(\sqrt{\frac{3}{4f(1-f)} + \frac{9p^4}{16\pi\rho_0 b^3}} - \sqrt{\frac{3}{4f(1-f)}})$ and taking $\chi_0 = \frac{\alpha}{T} + \beta$, we can solve this equation for *T*. Results from such calculations are shown in Figure 12, confirming that DOT increases significantly after oxidation. In addition, enhanced phase segregation is predicted if we compute domain spacing in the strong segregation limit by using the relation $\frac{d}{d_0} = (1 + \frac{p^4}{16\pi\rho_0\chi_0 b^3})^{1/6}$. Overall, these results confirm that indeed mismatch in dipole moments of two segments is an effective strategy toward high-χ copolymers.

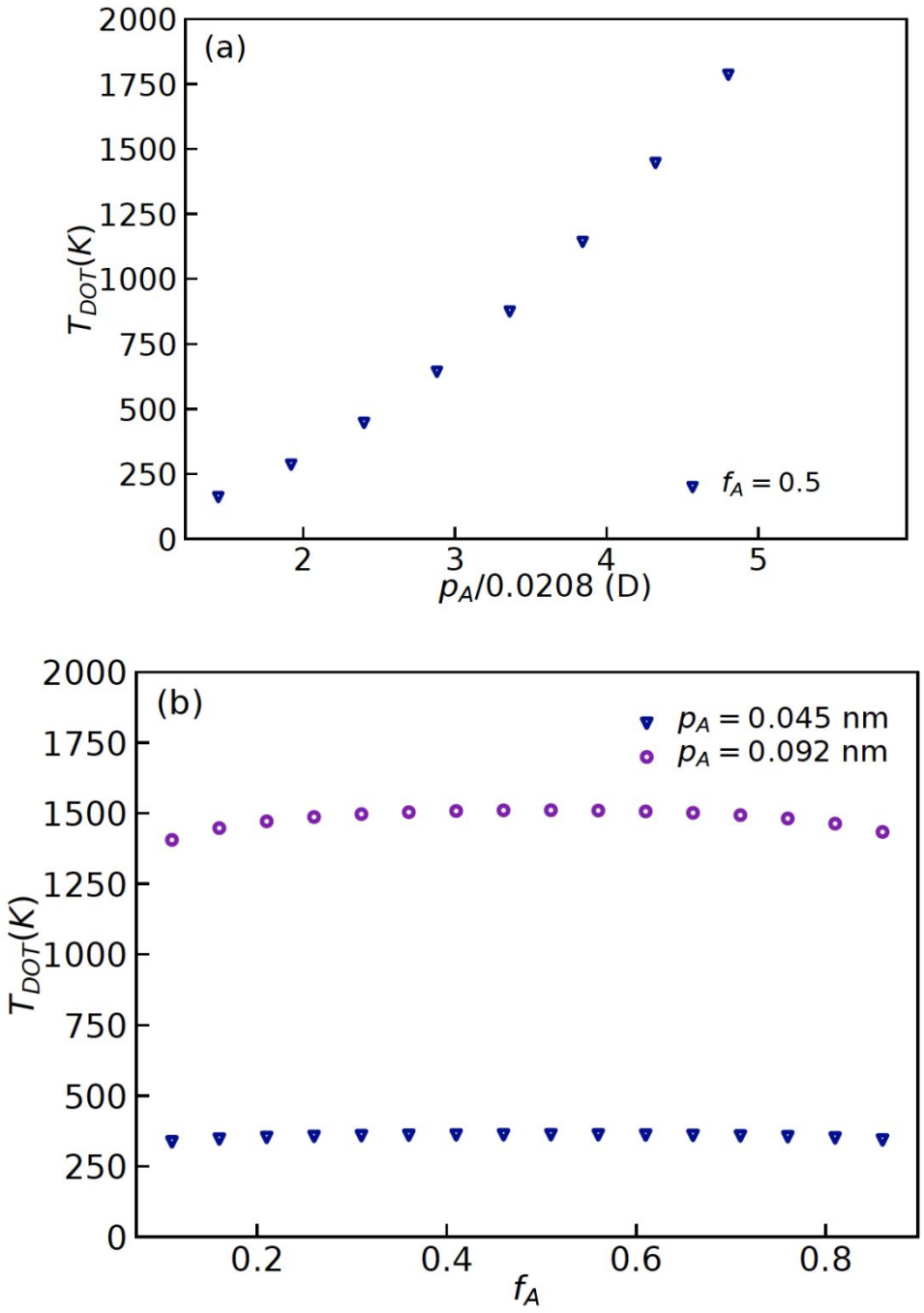

Figure 12. a) Calculated disorder-order transition temperature (T_{DOT}) as a function of (a) the dipole length (p_A) of polar segment A, and (b) fraction (f_A) of the polar block A. Panel b) corresponds to PS-P2VP (p_A = 0.045 nm) and PS-P2VPNO (p_A = 0.092 nm) diblock. Dipole length of the PS segment is taken to be zero. Above $T_{DOT,}$ disordered phase

is stable, and these results highlight that mismatch in dipole moments of two segments leads to enhanced segregation strength.

Conclusions

Block copolymers bearing polystyrene and poly(vinylpyridine N-oxides) segments, PS-*b*-P4VPNO and PS-*b*-P2VPNO, were successfully synthesized by anionic polymerizations followed by oxidation with glacial acetic acid and hydrogen peroxide. These block copolymers were thoroughly characterized and show highly amphiphilic characteristics. Thermal properties illustrated that poly(vinylpyridine N-oxide)s were thermally stable up to 220 ^{o}C, while no glass transition temperatures were observed before degradation, reflecting their polar features.

The self-assembly of these copolymers revealed high immiscibility among the blocks. For low molecular weight parent copolymers, disordered structures were mostly observed, while SAXS and AFM data showed the oxidized analogues formed various self-assembled structures, dictated by their compositions, and influenced by sample preparation conditions. Remarkably, PS_{34}-*b*-$P4VPNO_{27}$ with symmetric volume fraction showed cylindrical structures, demonstrating high-χ characteristics. The lack of order-disorder transition temperatures prohibited us from obtaining χ parameter using common methods. Based on the theory regarding permanent dipoles in a block copolymer affecting the χ parameter (thus their phase-separating behavior), using poly(vinylpyridine N-oxides) block in amphiphilic block copolymers was an effective approach toward high-χ copolymers. Our results demonstrate that PVPNO based block copolymers are versatile candidates toward nanopatterned structures with small feature sizes critical for the future microelectronics industry. Advanced functional materials based on these PVP derivatives are also potentially important in other applications, such as membrane materials, sensors, and detergent industries.

Acknowledgements

This research was conducted at the Center for Nanophase Materials Sciences (CNMS), which is a US Department of Energy, Office of Science User Facility at Oak Ridge National

Laboratory. We are extremely grateful to Dr. Steven Randolph (HIM), Dr. Dale Hensley (SEM), Dr. Yangyang Wang (BSD), Dr. Jihua Chen (TEM). Dr. Alexis Williams (TEM), and Dr. Martí Checa (AFM) from CNMS for their invaluable help and great efforts in characterizing these self-assembled block copolymers. We would also like to thank Dr. Peter Bonnessen for his help with 2D-NMR experiments and experiments done with hexafluoro-isopropanol-d2 (HFIP-d2) as solvent.

References:

1 L. Leibler, *Macromolecules*, 1980, **13**, 1602–1617.

2 H. C. Kim, S. M. Park and W. D. Hinsberg, *Chem. Rev.*, 2010, **110**, 146–177.

3 F. S. Bates and G. H. Fredrickson, *Annu. Rev. Phys. Chem.*, 1990, **41**, 525–557.

4 A. Blanazs, S. P. Armes and A. J. Ryan, *Macromol. Rapid Commun.*, 2009, **30**, 267–277.

5 W. Wang, W. Lu, A. Goodwin, H. Wang, P. Yin, N. G. Kang, K. Hong and J. W. Mays, *Prog. Polym. Sci.*, 2019, **95**, 1–31.

6 C. Li, Q. Li, Y. V. Kaneti, D. Hou, Y. Yamauchi and Y. Mai, *Chem. Soc. Rev.*, 2020, **49**, 4681–4736.

7 H. Feng, X. Lu, W. Wang, N. G. Kang and J. W. Mays, *Polymers (Basel).*, 2017, **9**, 494.

8 P. D. Topham, A. J. Parnell and R. C. Hiorns, *J. Polym. Sci. Part B Polym. Phys.*, 2011, **49**, 1131–1156.

9 C. Lang, M. Kumar and R. J. Hickey, *Soft Matter*, 2021, **17**, 10405–10415.

10 K. Brassat, D. Kool, J. Bürger and J. K. N. Lindner, *Nanoscale*, 2018, **10**, 10005–10017.

11 C. Park, J. Yoon and E. L. Thomas, *Polymer (Guildf).*, 2003, 44, 6725–6760.

12 M. W. Matsen and M. D. Whitmore, *J. Chem. Phys.*, 1996, **105**, 9698–9701.

13 C. Sinturel, F. S. Bates and M. A. Hillmyer, *ACS Macro Lett.*, 2015, **4**, 1044–1050.

14 C. Cummins, R. Lundy, J. J. Walsh, V. Ponsinet, G. Fleury and M. A. Morris, *Nano Today*, 2020, **35**, 100936.

15 P. P. Angelopoulou, I. Moutsios, G. M. Manesi, D. A. Ivanov, G. Sakellariou and A. Avgeropoulos, *Prog. Polym. Sci.*, 2022, 135, 101625.

16 G. Jeong, D. M. Yu, J. K. D. Mapas, Z. Sun, J. Rzayev and T. P. Russell, *Macromolecules*, 2017, **50**, 7148–7154.

17 P. P. Angelopoulou, M. M. Stathouraki, J. K. Keum, K. Hong, A. Avgeropoulos and G. Sakellariou, *Eur. Polym. J.*, 2023, **190**, 111995.

18 J. G. Kennemur, L. Yao, F. S. Bates and M. A. Hillmyer, *Macromolecules*, 2014, **47**, 1411–1418.

19 L. M. Pitet, S. F. Wuister, E. Peeters, E. J. Kramer, C. J. Hawker and E. W. Meijer, *Macromolecules*, 2013, **46**, 8289–8295.

20 M. D. Rodwogin, C. S. Spanjers, C. Leighton and M. A. Hillmyer, *ACS Nano*, 2010, **4**, 725–732.

21 J. D. Cushen, C. M. Bates, E. L. Rausch, L. M. Dean, S. X. Zhou, C. G. Willson and C. J. Ellison, *Macromolecules*, 2012, **45**, 8722–8728.

22 K. Azuma, J. Sun, Y. Choo, Y. Rokhlenko, J. H. Dwyer, B. Schweitzer, T. Hayakawa, C. O. Osuji and P. Gopalan, *Macromolecules*, 2018, **51**, 6460–6467.

23 W. Zhang, M. Huang, S. Al Abdullatif, M. Chen, Y. Shao-Horn and J. A. Johnson, *Macromolecules*, 2018, **51**, 6757–6763.

24 J. Kwak, A. K. Mishra, J. Lee, K. S. Lee, C. Choi, S. Maiti, M. Kim and J. K. Kim,

Macromolecules, 2017, **50**, 6813–6818.

25 A. K. Mishra, J. Lee, S. Kang, E. Kim, C. Choi and J. K. Kim, *Macromolecules*, 2022, **55**, 10797–10803.

26 G. Pino, C. Cummins, D. Mantione, N. Demazy, A. Alvarez-Fernandez, S. Guldin, G. Fleury, G. Hadziioannou, E. Cloutet and C. Brochon, *Macromolecules*, 2022, **55**, 6341–6350.

27 E. Hancox, M. J. Derry, M. J. Greenall, S. Huband, L. Al-Shok, J. S. Town, P. D. Topham and D. M. Haddleton, *Chem. Sci.*, 2022, **13**, 4019–4028.

28 Q. P. Chen, L. Barreda, L. E. Oquendo, M. A. Hillmyer, T. P. Lodge and J. I. Siepmann, *ACS Nano*, 2018, **12**, 4351–4361.

29 S. P. Ding, Z. K. Zhang, Z. Ye, B. Y. Du and J. T. Xu, *ACS Macro Lett.*, 2021, **10**, 1321–1325.

30 J. Park, A. Staiger, S. Mecking and K. I. Winey, *ACS Nano*, 2021, **15**, 16738–16747.

31 J. G. Kennemur, *Macromolecules*, 2019, 52, 1354–1370.

32 J. M. J. Fréchet and M. V. de Meftahi, *Br. Polym. J.*, 1984, **16**, 193–198.

33 D. Lee, J. Kim, K. H. Ku, S. Li, J. J. Shin and B. J. Kim, *Polym. Chem.*, 2022, **13**, 2570–2588.

34 D. L. Comins, S. O'Connor and R. S. Al-Awar, in *Comprehensive Heterocyclic Chemistry III*, Elsevier, 2008, vol. 7, pp. 41–99.

35 N. Volk, D. Vollmer, M. Schmidt, W. Oppermann and K. Huber, in *Advances in Polymer Science: Polyelectrolytes with Defined Molecular Architecture II*, Springer, Berlin, Heidelberg, 2004, vol. 166, pp. 29–65.

36 K. Mavronasou, A. Zamboulis, P. Klonos, A. Kyritsis, D. N. Bikiaris, R. Papadakis and I. Deligkiozi, *Polymers (Basel).*, 2022, **14**, 804.

37 J. Meisenheimer, *Berichte der Dtsch. Chem. Gesellschaft (A B Ser.*, 1926, **59**,

1848–1853.

38 F. E. Cislak, *Ind. Eng. Chem.*, 1955, **47**, 800–802.

39 A. R. Katritzky and J. N. Lam, *Heterocycles*, 1992, **33**, 1011–1049.

40 D. Li, P. Wu, N. Sun, Y.-J. Lu, W.-L. Wong, Z. Fang and K. Zhang, *Curr. Org. Chem.*, 2019, **23**, 616–627.

41 T. Tamikado, T. Sakai and K. Sagisaka, *Die Makromol. Chemie*, 1961, **50**, 244–252.

42 S. Goldstein, G. Czapski and A. Heller, *Chem. Res. Toxicol.*, 2006, **19**, 86–91.

43 P. F. Holt, H. Lindsay and E. T. Nasrallah, *Nat.* , 1967, **216**, 611–612.

44 L. Gregson and P. Holt, *Die Makromol. Chemie*, 1969, **128**, 193–196.

45 W. Maul, *J. Labelled Compd.*, 1968, **4**, 350–355.

46 B. Tamami and N. Goudarzian, *Eur. Polym. J.*, 1992, **28**, 1035–1038.

47 A. M. Bauer, E. E. Ramey, K. G. Oberle, G. A. Fata, C. D. Hutchison and C. R. Turlington, *Tetrahedron Lett.*, 2019, **60**, 151193.

48 Z. Wrzeszcz and R. Siedlecka, *Molecules*, 2020, **25**, 330.

49 H. Wang, Y. Fan and Y. Wang, *J. Surfactants Deterg.*, 2017, **20**, 647–657.

50 M. Beneito-Cambra, J. M. Herrero-Martínez and G. Ramis-Ramos, *Electrophoresis*, 2008, **29**, 3245–3252.

51 M. N. Amin and R. S. Blackburn, *ACS Sustain. Chem. Eng.*, 2015, **3**, 725–732.

52 R. Shevate, M. Karunakaran, M. Kumar and K. V. Peinemann, *J. Memb. Sci.*, 2016, **501**, 161–168.

53 R. Zeng, Z. Gong, L. Chen and Q. Yan, *ACS Macro Lett.*, 2020, **9**, 1102–1107.

54 D. Uhrig and J. W. Mays, *J. Polym. Sci. Part A Polym. Chem.*, 2005, **43**, 6179–6222.

55 N. Hadjichristidis, H. Iatrou, S. Pispas and M. Pitsikalis, *J. Polym. Sci. Part A Polym. Chem.*, 2000, **38**, 3211–3234.

56 E. Ochiai, *J. Org. Chem.*, 1953, **18**, 534–551.

57 S. Biggs and B. Vincent, *Colloid Polym. Sci.*, 1992, **270**, 505–510.

58 W. Zha, C. D. Han, D. H. Lee, S. H. Han, J. K. Kim, J. H. Kang and C. Park, *Macromolecules*, 2007, **40**, 2109–2119.

59 D. Y. Ryu, U. Jeong, D. H. Lee, J. Kim, H. S. Youn and J. K. Kim, *Macromolecules*, 2003, **36**, 2894–2902.

60 E. F. V. Scriven, in *Comprehensive Heterocyclic Chemistry*, Elsevier Inc., 1984, vol. 2, pp. 165–314.

61 N. Sakamoto, H. Tanaka, K. Yamaguchi, M. Yoshida and S. Arichi, *Die Makromol. Chemie*, 1985, **186**, 1881–1894.

62 P. F. Holt and H. Lindsay, *J. Chem. Soc. B Phys. Org.*, 1969, 54–61.

63 P. F. Holt and E. T. Nasrallah, *J. Chem. Soc. B Phys. Org.*, 1968, 233–237.

64 C. M. Lee, E. M. Pearce and T. K. Kwei, *Polymer (Guildf).*, 1996, **37**, 4283–4288.

65 A. Clark, M. Rosenbaum, Y. Biswas, A. Asatekin and P. Cebe, *Polymer (Guildf).*, 2022, **256**, 125176.

66 C. Sinturel, M. N. Vayer, M. Morris and M. A. Hillmyer, *Macromolecules*, 2013, **46**, 5399–5415.

67 M. C. D. Carter, J. Jennings, F. W. Speetjens, D. M. Lynn and M. K. Mahanthappa, *Macromolecules*, 2016, **49**, 6268–6276.

68 N. P. Young and N. P. Balsara, in *Encyclopedia of Polymeric Nanomaterials*, Springer Berlin Heidelberg, 2015, pp. 747–755.

69 S. Sakurai, K. Mori, A. Okawara, K. Kimishima and T. Hashimoto, *Evaluation of Segmental Interaction by Small-Angle X-ray Scattering Based on the Random-Phase Approximation for Asymmetric, Polydisperse Triblock Copolymers*, 1992,

vol. 25.

70 W. J. Durand, G. Blachut, M. J. Maher, S. Sirard, S. Tein, M. C. Carlson, Y. Asano, S. X. Zhou, A. P. Lane, C. M. Bates, C. J. Ellison and C. G. Willson, *J. Polym. Sci. Part A Polym. Chem.*, 2015, **53**, 344–352.

71 J. M. Kim, Y. H. Hur, J. W. Jeong, T. W. Nam, J. H. Lee, K. Jeon, Y. Kim and Y. S. Jung, *Chem. Mater.*, 2016, **28**, 5680–5688.

72 A. H. Hofman, G. O. R. Alberda Van Ekenstein, A. J. J. Woortman, G. Ten Brinke and K. Loos, *Polym. Chem.*, 2015, **6**, 7015–7026.

73 C. J. Clarke, A. Eisenberg, J. La Scala, M. H. Rafailovich, J. Sokolov, Z. Li, S. Qu, D. Nguyen, S. A. Schwarz, Y. Strzhemechny and B. B. Sauer, *Macromolecules*, 1997, **30**, 4184–4188.

74 R. Kumar, W. Li, B. G. Sumpter and M. Muthukumar, *J. Chem. Phys.*, 2019, **151**, 054902.